Tunneling from Electronic Bubble States in Liquid Helium through the Liquid-Vapor Interface

W. Schoepe* and G. W. Rayfield†
Department of Physics, University of Oregon, Eugene, Oregon 97403
(Received 29 December 1972)

The escape of electrons from their bubble state in liquid helium through the free liquid surface into the vapor phase is investigated. The measured escape rates are calculated in terms of a tunneling model which predicts a unique temperature and electric field dependence in excellent agreement with the experimental data. A fit of this model to the data yields the binding energy and the radius of the electronic bubble. The binding energy is found to be 0.70 eV in pure He^4 and 0.56 eV in pure He^3. The bubble radii are found to scale according to the bubble model; however, their absolute values appear to be too large. The results obtained from two different He^3-He^4 mixtures are anomalous and not yet understood.

I. INTRODUCTION

The transport of charges through dielectric liquids has been extensively used to study the properties of the liquid state as well as the nature of the charge carriers. The most important example is liquid helium. The repulsive electron-helium interaction leads to a bubble state for a thermalized excess electron. The positive charge carrier, which is created in liquid helium by means of ionizing radiation, is generally considered to be a helium ion, He_2^+, surrounded by a cluster of polarized helium atoms. The transport properties of these structures are governed by their interaction with the elementary excitations of the liquid.[1] Measurements of the mobility,[2] the charge trapping in quantized vortex lines,[3] and photoexcitation[4] of electronic bubble states have yielded insight into the structure of the excess electron in liquid helium. In a completely different type of experiment a striking difference between positive ions and electron bubbles was observed. It was found that positive ions could not be extracted through the free surface of liquid helium into the vapor phase, whereas negative ions (electronic bubbles) could pass through the liquid-vapor interface quite easily, provided the temperature was not too low.[5,6] Evidently the structure of the charge carriers plays a key role in the evaporation process.

Early measurements of the temperature dependence of a dc electron current through the free surface of liquid He^4 into the vapor indicated a potential barrier caused by the repulsive image force below the surface.[5,7] This image potential in combination with an externally applied electric field normal to the interface leads to a potential well below the surface, which traps the charges for extended periods of time.[8] We have measured these trapping times τ as a function of temperature and electric field. An analysis of our data in terms of a classical diffusion model[8] resulted in several difficulties. Whereas the temperature dependence seemed to be given correctly, the electric field dependence of the trapping times was only in fair agreement with the data. Furthermore, the required cutoff of the image potential close to the surface turned out to be extremely sharp, thereby violating an underlying assumption of Smoluchowski's equation which applies only for a slowly varying potential. These circumstances led us to a different model, which describes the escape of the electrons through the free liquid surface as a tunneling process from their ground state inside the bubble into the vapor phase.[9] The escape probability $P = \tau^{-1}$ was found from the model to depend exponentially on two important parameters of the bubble state—namely, the radius and the binding energy—both of which can be determined from a fit of the experimental data to this model. Since no superfluid properties are involved, these experiments can be performed in all dielectric liquids in which electronic bubble states exist with a positive ground-state energy. So far we have investigated only He^4, He^3, and some He^3-He^4 mixtures. Our results for the radius and the binding energy of electronic bubble states in these liquids were communicated recently in a short report.[10]

Section II describes our theoretical model for the escape probability P and Sec. III contains experimental details. Our data are presented and evaluated in Sec. IV. We discuss our results in Sec. V, and in Sec. VI we mention some conclusions and speculations. In the Appendix we elaborate on some details of the investigations.

II. CALCULATION OF ESCAPE PROBABILITY

As the electron bubble approaches the free liquid surface, it encounters a potential well which results from the applied electric field $\mathcal{E}$ normal to the surface, and the repulsive interaction of the electron with its image above the interface[8]:

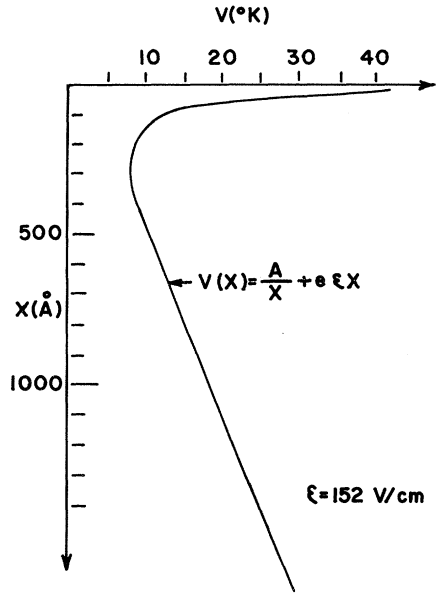

FIG. 1. Image-induced potential well which traps particles just below the free surface.

$$V(x) = A/x + e\mathcal{E}x, \quad A = e^2(\epsilon - 1)/4\epsilon(\epsilon + 1) ,$$

where x is the distance from the surface, e the electronic charge, and ϵ the dielectric constant of the liquid (see Fig. 1). This form of the potential holds up to few angstroms below the surface, where it breaks down owing to the finite density profile of the interface. Assume that N_0 ions are introduced into the well at a time $t = 0$ and that each ion is independent of all the other ions in the well. The number of ions which escape per unit time dN/dt is then proportional to the number $N(t)$ in the well:

$$\frac{dN}{dt} = -PN(t) ,$$

where P is the escape probability per unit time. Hence

$$N(t) = N_0 e^{-Pt} .$$

Thus the current from the surface is

$$j_s = -\frac{dN}{dt} = PN(t) = PN_0 e^{-Pt} .$$

We now proceed to calculate P by describing the escape of the electron from the liquid as a tunneling process from the ground state inside the bubble into the vapor phase. The barrier height through which the electron must tunnel is $E_1 - E_0$, where E_1 is the lowest energy a quasifree electron can have in the liquid (edge of the "conduction band") and E_0 is the ground-state energy inside the bubble (see Fig. 2). For convenience, we set

$$E_1 - E_0 = \hbar^2 \alpha^2 / 2m_e ,$$

m_e being the mass of the electron. If the center of the bubble is at a distance x from the surface, the barrier width is $d = x/\cos\theta - R$ (see Fig. 2), where R is the bubble radius. We will neglect surface and bubble distortions in the present calculation. The probability the electron tunnels a distance d through the liquid is taken to be $e^{-2\alpha d}$.[11] The tunneling transition rate from the bubble at the solid angle $d\Omega$ is

$$\nu \exp\left[-2\alpha\left(\frac{x}{\cos\theta} - R\right)\right] \frac{d\Omega}{4\pi} ,$$

where ν in a semiclassical sense is the frequency with which the electron "hits" the walls of the bubble $[\nu \approx (2E_0/m_e)^{1/2}/2R]$. The total transition rate is

$$\tfrac{1}{2}\nu \int_0^{\pi/2} \exp\left[-2\alpha\left(\frac{x}{\cos\theta} - R\right)\right] \sin\theta \, d\theta$$

$$= \tfrac{1}{2}\nu e^{2\alpha R} W(x) , \quad (1)$$

where

$$W(x) = e^{-2\alpha x} + 2\alpha x \, \mathrm{Ei}(-2\alpha x) ,$$

Ei being the exponential integral. In our regions of interest we always have $2\alpha x \gg 1$. We approximate Ei for large argument[12]

$$2\alpha x \, \mathrm{Ei}(-2\alpha x) = -e^{-2\alpha x}[1 - 1/2\alpha x + 2/(2\alpha x)^2 - \cdots] .$$

Neglecting terms of third order and higher, we obtain

$$W(x) \approx \frac{e^{-2\alpha x}}{2\alpha x}\left(1 - \frac{1}{\alpha x}\right) .$$

In general, the second term in the parentheses can also be dropped. We found, however, a slight improvement of the calculation by replacing the expression in the parentheses by $e^{-1/\alpha x}$, i.e.,

$$W(x) \approx (e^{-2\alpha x}/2\alpha x)\, e^{-1/\alpha x} . \quad (2)$$

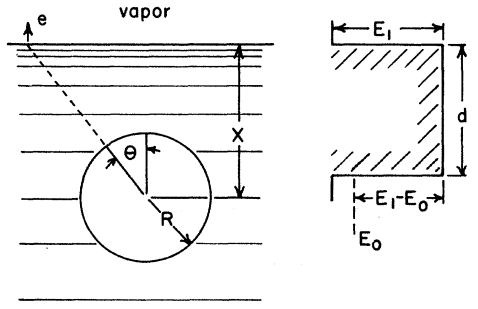

FIG. 2. Tunneling from an electron bubble located a distance x from the free surface. The potential barrier $E_1 - E_0$ through which the electron tunnels is also shown. E_0 is the ground-state energy of the electron inside the bubble.

If the number of electronic bubbles between x and $x+dx$ is $n(x)dx$, the current through the surface from the region is $\frac{1}{2}\nu e^{2\alpha R} W(x)n(x)dx$. Rigorously, Smoluchowski's diffusion equation should now be solved for $n(x)$. In the Appendix, this problem will be discussed in greater detail. The observed escape rate of the electrons in the potential $V(x)$ is of the order of seconds and the relaxation of the ions to thermal equilibrium is of the order of 10^{-10} sec. It is reasonable to assume, therefore, an equilibrium distribution (Maxwell–Boltzmann) throughout the potential well.[13] We set

$$n(x) = C e^{-V(x)/T} .$$

The normalization constant C is determined by the condition

$$\int_0^\infty n(x)\,dx = N ,$$

where N is the total number of particles in the well at some particular time. We obtain

$$C = N/I_1 ,$$

with

$$I_1 = \int_0^\infty e^{-V(x)/T}\,dx = 2\left(\frac{A}{e\mathcal{E}}\right)^{1/2} \times K_1\left(\frac{2(Ae\mathcal{E})^{1/2}}{T}\right) \text{ Å} .$$

Our units are the same as those of our previous work,[9] K_1 is a modified Bessel function.[14] The total current j_s from the surface is then given by

$$j_s = PN = \tfrac{1}{2}\nu e^{2\alpha R}\int_0^\infty n(x)W(x)\,dx = \tfrac{1}{2}\nu e^{2\alpha R} N(I_2/I_1) , \quad (3)$$

where

$$I_2 = \int_0^\infty \left\{\exp\left[-\left(\frac{A}{Tx} + \frac{e\mathcal{E}x}{T} + 2\alpha x + \frac{1}{\alpha x}\right)\right]\right\}\Big/ 2\alpha x\,dx .$$

We have extended the lower integration boundary of I_1 and I_2 from $x=R$ to $x=0$, which can be done without introducing a significant error, because of the steep fall of $n(x)$ for $x \to 0$. The integral I_2 is given by another modified Bessel function[14]:

$$I_2 = \alpha^{-1} K_0(Z) \text{ Å} ,$$

with

$$Z = \left[4\left(\frac{A}{T} + \frac{1}{\alpha}\right)\left(2\alpha + \frac{e\mathcal{E}}{T}\right)\right]^{1/2} .$$

Finally, for the escape probability P, we obtain

$$P = \frac{j_s}{N} = \frac{1}{2}\nu e^{2\alpha R}\frac{I_2}{I_1} = \frac{1}{2}\nu e^{2\alpha R} K_0\left\{\left[4\left(\frac{A}{T} + \frac{1}{\alpha}\right)\left(2\alpha + \frac{e\mathcal{E}}{T}\right)\right]^{1/2}\right\}\Big/ 2\alpha\left(\frac{A}{e\mathcal{E}}\right)^{1/2} K_1\left(\frac{2(Ae\mathcal{E})^{1/2}}{T}\right) . \quad (4)$$

An estimate of the arguments of K_0 and K_1 in Eq. (4) indicated that they are large enough to allow the following approximation[15] for the Bessel functions:

$$K_0(Z) \approx (\pi/2Z)^{1/2} e^{-Z} ,$$

$$K_1(Y) \approx \left(\frac{\pi}{2Y}\right)^{1/2} e^{-Y}\left(1 + \frac{3}{8Y}\right) .$$

Furthermore, we can set

$$Z = \left[\frac{8A\alpha}{T}\left(1 + \frac{T}{A\alpha}\right)\right]^{1/2}\left(1 + \frac{e\mathcal{E}}{2\alpha T}\right)^{1/2} \approx \left(\frac{8A\alpha}{T}\right)^{1/2}\left(1 + \frac{T}{2A\alpha}\right)\left(1 + \frac{e\mathcal{E}}{4\alpha T}\right) .$$

Neglecting products of small terms, we obtain

$$Z \approx \left(\frac{8A\alpha}{T}\right)^{1/2} + \frac{e\mathcal{E}}{\alpha T}\left(\frac{A\alpha}{2T}\right)^{1/2} + \left(\frac{2T}{A\alpha}\right)^{1/2} .$$

In our case, the first term of the series is by far the largest. The two others can be considered as small corrections; we will take them into account where they appear as exponents. Using these approximations, we obtain

$$P(\alpha, R, \mathcal{E}, T) \approx \tfrac{1}{2}\nu e^{2\alpha R} G(\mathcal{E}, T) \times e^{2(Ae\mathcal{E})^{1/2}/T} e^{-(8A\alpha/T)^{1/2}} \text{ sec}^{-1} , \quad (5)$$

with

$$G(\mathcal{E}, T) = (e\mathcal{E})^{3/4}\left\{2^{5/4}\alpha^{5/4}T^{1/4}A^{1/2}\left(1 + \frac{3T}{16(Ae\mathcal{E})^{1/2}}\right) \times \exp\left[\frac{e\mathcal{E}}{\alpha T}\left(\frac{\alpha A}{2T}\right)^{1/2} + \left(\frac{2T}{\alpha A}\right)^{1/2}\right]\right\}^{-1} .$$

G depends weakly on α, but the dominant dependence of P is contained in the exponential functions in Eq. (5). We notice that we can obtain a universal temperature dependence of P for all $\mathcal{E}$ by normalizing

$$P/\gamma = \tfrac{1}{2}\nu e^{2\alpha R} e^{-(8A\alpha/T)^{1/2}} , \quad (6)$$

where

$$\gamma(\mathcal{E}, T) = G(\mathcal{E}, T) e^{2(Ae\mathcal{E})^{1/2}/T} .$$

From Eq. (6) we can determine α and R from a best fit to the experimentally measured values of P. The procedure will require few iterations, because of the weak influence of α on the otherwise computable function γ.

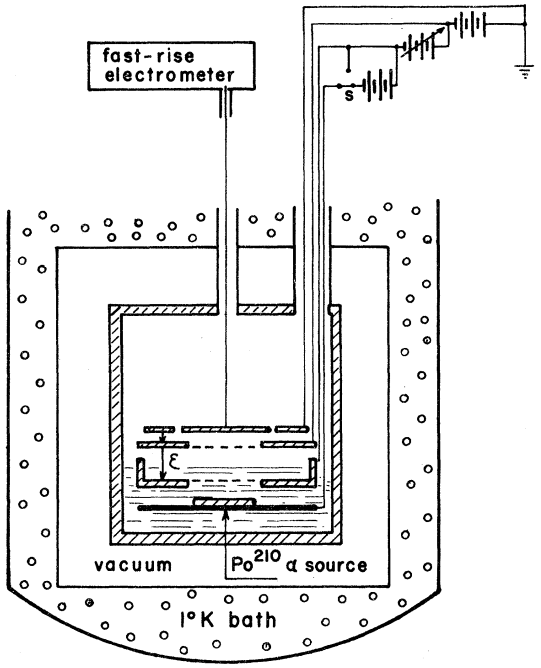

FIG. 3. Schematic diagram of the experimental cell.

III. EXPERIMENTAL DETAILS

The present experimental procedure to measure the trapping time $\tau = P^{-1}$ is essentially the same as the one we communicated earlier.[8] Figure 3 shows a schematic of the gold-plated measuring chamber. Charges were produced in the liquid by a radioactive source $S(^{210}\mathrm{Po})$. By applying suitable electric fields between S and grid G and between G and the Frisch grid F the liquid surface, which was located above G, could be charged. A guard ring attached to G prevented the surface charge from leaking to the walls of the cell. The current leaving the surface and arriving at the collector C was measured by an operational amplifier (Keithley 300). The voltage between S and G was then switched off while the electric field $\mathcal{E}$ across the surface and the temperature T were held constant. The exponential decay of the current (and hence of the surface charge) was recorded (see Fig. 4). Trapping times ranging from 0.4 up to 100 sec could be conveniently measured. The lower limit was determined by the rise time of the electrometer amplifier and the upper limit by its sensitivity (low escape rates produce only small currents). It should be mentioned that low escape rates can lead to a considerable pileup of surface charge which distorts the external electric field $\mathcal{E}$. In this case, the decay of the currents does not start exponentially. Only after the surface charge becomes small enough so as not to influence the applied electric field is an exponential decay observed.

We checked our new system by reproducing He^4 data taken in our earlier apparatus[8] above 1.2 °K. We then studied He^3 and He^3-He^4 mixtures. The lower required temperatures were achieved by cooling the chamber with a one-shot He^3 cryostat. The temperatures were measured with a germanium resistor located at the bottom of the cell.

IV. RESULTS

We first present our earlier results[8] for pure He^4 and analyze them in terms of the model described in Sec. II. Figure 5 shows the measured trapping times $\tau(\mathcal{E}, T) = P^{-1}(\mathcal{E}, T)$ as a function of temperature for different electric fields $\mathcal{E}$ across the free liquid surface. The abscissa is plotted linearly in T^{-1}, which results in an approximate straight-line behavior for $\ln\tau$ over a limited temperature interval. The solid lines are calculated from Eq. (5) by varying α and R for a best fit. The following procedure was used: According to Eq. (6) we can plot a universal curve $\ln(P/\gamma)$ vs $T^{-1/2}$ and obtain α from the slope. Because of the weak influence of the unknown quantity α on the function γ, few iterations are necessary. Starting with an estimated α, we get a stable value after three iterations. The resulting universal curve for He^4 is shown in Fig. 6. α determines the slope of the curve and R can be then obtained from the intercept. The weak dependence of the frequency ν on R is no problem here because it is dominated by the exponential R dependence in Eq. (6). Taking an image-potential coefficient $A = 1099$ °K Å derived

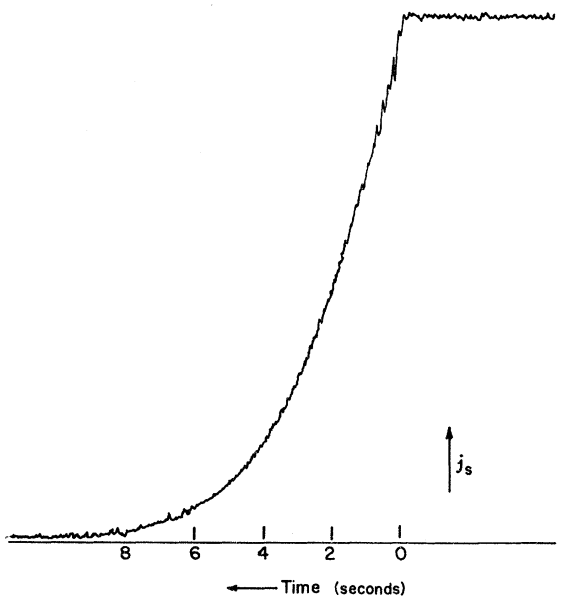

FIG. 4. Exponential decay of the surface current when the ion source is switched off.

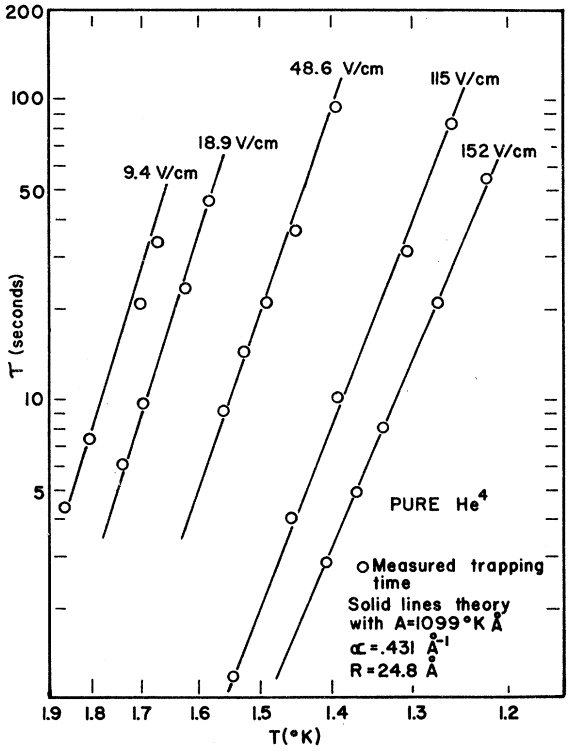

FIG. 5. Experimental measured trapping times τ as a function of temperature T for pure He^4. τ varies from about 1 to 100 sec.

from the dielectric constant $\epsilon = 1.057$,[16] we obtain, from Fig. 6, $\alpha = 0.431$ Å^{-1} and $R = 24.8$ Å.[17] With these results the solid lines in Fig. 5 were calculated from Eq. (5). It is interesting that the value of A can also be determined directly from the experimental data. This is discussed in detail at the end of this section.

The results obtained by applying the same procedure to pure He^3 are shown in Figs. 7 and 8. Taking $A = 837$ °K Å calculated from $\epsilon = 1.042$,[18] we obtain, from Fig. 8, $\alpha = 0.384$ Å^{-1} and $R = 30.1$ Å. With these values, Eq. (5) gives the solid lines shown in Fig. 7. The trapping times are considerably shorter for equal temperatures and fields than in He^4. Therefore, we had to take our data at lower temperatures by cooling the sample in the He^3 cryostat. The experimental results again can be described nicely by Eqs. (5) and (6), as can be seen in Figs. 7 and 8. The universal curve in Fig. 8 shows the predicted straight-line behavior for $\ln(P/\gamma)$ vs $T^{-1/2}$ even though P/γ changes by five orders of magnitude.

In Fig. 9 our data for two He^3-He^4 mixtures are shown together with those obtained in the pure liquids. Two pecularities of the mixture are evident. First, a straight-line behavior of the data in Fig. 9 holds only above 1 °K. From these portions of the curves we obtain for the 19.5% mixture $\alpha = 0.232$ Å^{-1} and $R = 21.7$ Å, and for the 12% mixture

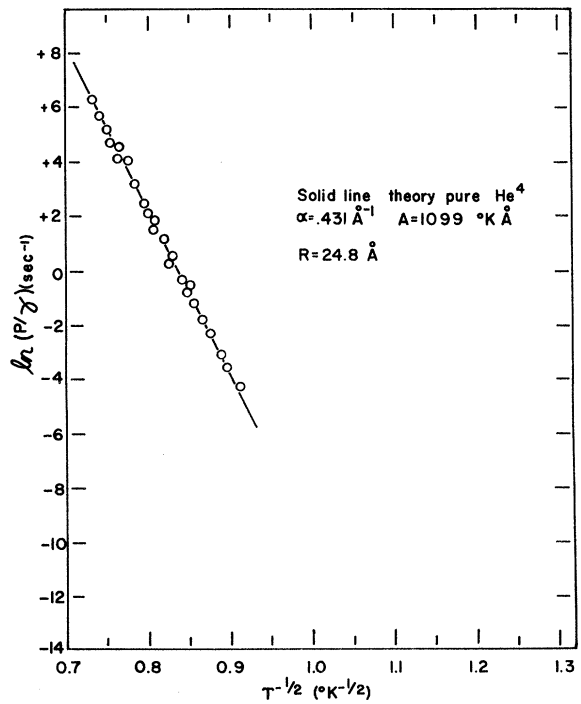

FIG. 6. $\ln(P/\gamma)$ vs $T^{-1/2}$ for pure He^4, where $P = 1/\tau$ and γ is defined in the text.

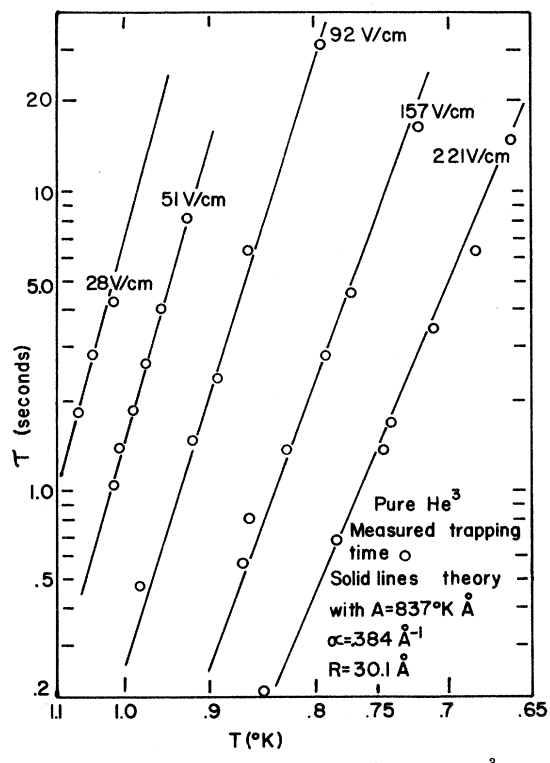

FIG. 7. Trapping time τ vs T for pure He^3.

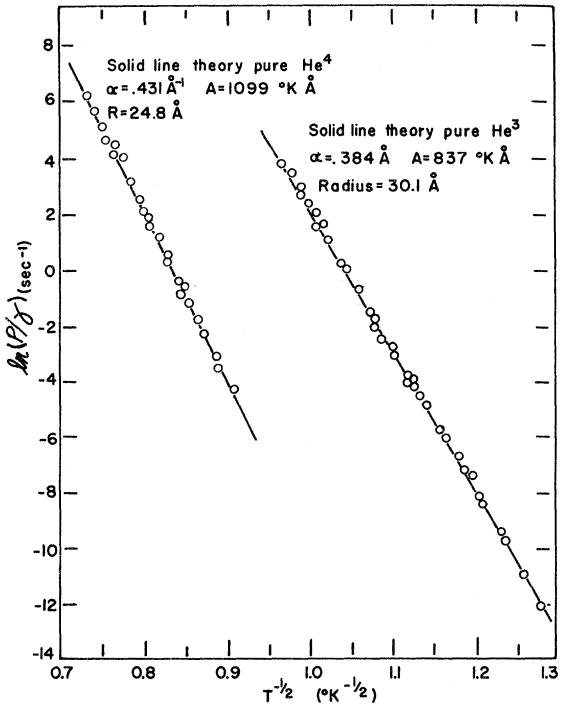

FIG. 8. $\ln(P/\gamma)$ vs $T^{-1/2}$ for pure He^3 and pure He^4.

$\alpha = 0.298$ Å^{-1} and $R = 23.6$ Å. These values are below those of the pure liquids, and not between as one might have expected. Second, at lower temperatures there is a strong deviation from the straight-line behavior. In fact, the trapping time in the 19.5% mixture was found to go through a maximum near 0.6 °K (at $\mathcal{E} = 263$ V/cm) and to decrease if the temperature is lowered to 0.48 °K. In the 12% solution, the deviation from the straight line is much smaller, and no maximum was found above 0.478 °K. In the 12% mixture, the plot of $\ln(P/\gamma)$ vs $T^{-1/2}$ fits a straight line over a range of eight orders of magnitude in P/γ. The general form of Eqs. (5) and (6) seems to be valid for the 12% mixture down to $T = 0.9$ °K.

Below 0.6 °K another unexpected observation was made. After the source voltage was switched off, the current first dropped very fast and only after about 40 sec was a well-defined exponential decay recorded. This behavior cannot be attributed to the influence of space-charge fields described in Sec. III, since they produce the opposite effect on the time decay of the current. An analysis of the decay curves indicates that a second decay constant might be present (which is about 10 sec) and which does not change appreciably down to 0.48 °K. However, within the first 10 sec, the decay is still too sharp to be fitted by these two exponentials. No attempts were made to fit these curves to other functions. It should also be mentioned that this unexpected behavior of the mixtures was associated with a strong increase of the dc currents from the surface as the temperature was lowered.

Before we start to discuss our results, we can check whether the theoretical value for the image-potential coefficient $A = e^2(\epsilon - 1)/4\epsilon(\epsilon + 1)$ which we used is in agreement with our data. This was done by analyzing the $\mathcal{E}$ dependence of the trapping times in the following way. The dominant $\mathcal{E}$ dependence is given by the factor $e^{2(Ae\mathcal{E})^{1/2}/T}$ in Eq. (5). The function $G(\mathcal{E}, T)$ can be computed because it does not depend very much on A (the absolute value of G, which depends on $A^{1/2}$, is presently not of interest). The factor $e^{-(8A\alpha/T)^{1/2}}$ is known from the curves in Fig. 9. From Eq. (5) we therefore can calculate

$$P/\beta = \tfrac{1}{2}\nu e^{2\alpha R} e^{2(Ae\mathcal{E})^{1/2}/T}, \tag{7}$$

where $\beta = G(\mathcal{E}, T)e^{-(8A\alpha/T)^{1/2}}$. Taking the experimentally determined values for α, we can determine A from a plot of $\ln(P/\beta)$ vs $(e\mathcal{E})^{1/2}/T$, which should be a straight line. The resulting values for A deviate less than 2% from the ones previously calculated[19] using the known dielectric constants and assuming a flat liquid surface. It should be emphasized that only one set of values for A and

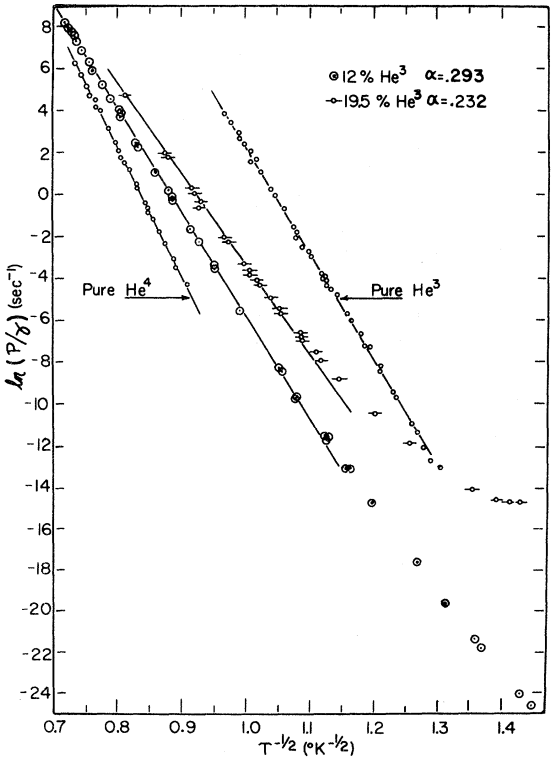

FIG. 9. $\ln(P/\gamma)$ vs $T^{-1/2}$ for two different He^3-He^4 mixtures and for pure He^4 and pure He^3.

TABLE I. Summary of the experimental results.

	$A=\frac{e^2(\epsilon-1)}{4\epsilon(\epsilon+1)}$ (°K Å)		α	$E_1-E_0=\frac{\hbar^2\alpha^2}{2m_e}$	R
	Experiment	Theory	(Å^{-1})	(eV)	(Å)
pure He^4	1085	1099	0.431	0.70	24.8
12% He^3		1069	0.298		23.6
19.5% He^3		1047	0.232		21.7
pure He^3	833	837	0.384	0.56	30.1

α can describe both the $\mathcal{E}$ and T dependence of our data correctly. Therefore, our assumption for the image-induced potential $V(x)=A/x+e\mathcal{E}x$ with $A=e^2(\epsilon-1)/4\epsilon(\epsilon+1)$ is justified.

Our results are summarized in Table I. The accuracy of the results depends on the accuracy with which the straight lines in Fig. 9 can be determined, i.e., about 1%. Hence E_1-E_0 may have an error of about 4%.

V. DISCUSSION

In this section we shall discuss our results for the binding energy E_1-E_0 and the radius R of the electronic bubble states in liquid helium. A comparison will be made with corresponding values obtained from other experiments and from theoretical calculations. We shall also consider some difficulties and obvious shortcomings of our theoretical model presented in Sec. II.

There are several theoretical approaches to calculate the energy of a quasifree electron in liquid helium. Burdick[20] investigated the propagation of an electron in an unperturbed regular lattice of He atoms. The ground-state energy turned out to be insensitive to the particular lattice selected. For a density corresponding to that of liquid He^4 he finds an energy $E_1=1.1$ eV, and $E_1=0.78$ eV for He^3. Other authors[21] have used the Wigner–Seitz approximation to calculate E_1, considering an atom as a hard sphere of radius a (the low-energy-electron scattering length) arranged in a periodic array with a Wigner–Seitz equivalent sphere radius r_s given by

$$\tfrac{4}{3}\pi r_s^3 n=1\ ,$$

where n is the number density of the liquid. Matching boundary conditions for s-like wave functions,

$$\frac{d}{dr}\left(\sin\frac{k(r-a)}{r}\right)_{r=r_s}=0\ ,$$

gives a condition for the wave number k_0 of the electron,

$$k_0 r_s=\tan k_0(r_s-a)\ ,$$

from which $E_1=\hbar^2k_0^2/2m_e$ can be computed. The results for He^4 indicate $E_1=1.3$ eV, and for He^3, $E_1=0.93$ eV, the uncertainties arising from the treatment of the polarization effects.[21]

Alternatively, an optical approximation has been used to study the problem.[22] In that model, the He atoms are considered as randomly distributed scattering centers. One finds that the liquid acts like a potential barrier of height

$$E_1=2\pi\hbar^2 an/m_e\ ,$$

where a is the scattering length and n the number density. It is interesting to note that this result agrees with the Wigner–Seitz result in the limit of low densities.[23] At liquid-helium densities, however, the optical model yields $E_1=0.6$ eV, i.e., about a factor of 2 less than the Wigner–Seitz model.

Recently Fetter[24] has improved the optical model by taking into account two-body correlations between the He atoms, the so-called shadowing effect. This approximation yields

$$E_1=\frac{2\pi\hbar^2 an}{m_e}\left(1-4\pi an\int_0^\infty rF(r)\,dr\right)$$
$$=\frac{2\pi\hbar^2 an}{m_e}(1+2\pi anr_s^2)\ ,$$

where $F(r)$ is the two-body correlation function. From this formula one obtains

$$E_1=0.87\text{ eV for }He^4$$
$$=0.64\text{ eV for }He^3\ .$$

So far, three different types of experiments have been performed in liquid He^4 from which the energy E_1 could be inferred. Sommer[25] injected electrons from the vapor phase into the liquid and found a required minimum energy of 1.3 eV for injection of the electrons, with an accuracy of about 30%. Woolf and Rayfield[26] measured the shift of the spectral response of a phototube after it was broken and filled with liquid He^4. They found the response curve to be shifted by 1.02 eV. There remains some doubt, however, whether this shift is really the change of the work function. Northby and Sanders[4] and Zipfel[4] studied the photoexcitation of electronic bubble states in liquid He^4. An interpretation of their data by Miyakawa and Dexter[27] yields $E_1=0.95$ eV. Details of this experiment are not clear to us, in particular, the role played by quantized vorticity.

In order to compare our results with the experimental and theoretical investigation above, we have to know the ground-state energy E_0 of the electron inside the bubble. Since E_0 is mostly determined by the bubble radius R (and rather insensitive to changes in E_1), we could compute E_0 from our measured values for R. However, as we will discuss below, our absolute values for R should not be taken too literally. We therefore prefer to compute E_0 in He^4 from the so far generally accepted value of $R=16$ Å, around which experimental evidence

has centered. Taking this value, we obtain $E_0 = 0.12$ eV from the simple bubble model. A recent attempt to measure this energy by a stopping-potential measurement at low temperatures gave a value 0.03 eV higher, corresponding to $R = 14$ Å.[28] Because of the difficulties inherent to that experiment, we continue to use the computed $E_0 = 0.12$ eV in He^4. No such data are available to calculate E_0 in He^3. The bubble model, however, predicts a relation between E_0 and the surface tension σ:

$$E_0 \propto \sigma^{1/2} .$$

Taking the known surface tensions,[29] we obtain $E_0 = 0.09$ in He^3. Combining these values with our experimental results, we finally get

$$E_1 = 0.82 \text{ eV for } He^4$$
$$= 0.65 \text{ eV for } He^3 .$$

We find a fair agreement with Fetter's optical model.[24]

We now turn to the discussion of the bubble radii. They were determined from the intercepts of the straight-line fits in Fig. 9. The value of 24.8 Å in He^4 is considerably larger than that derived from other experiments, e.g., ion trapping on vortex lines.[3] Since R determines the absolute value of the tunneling probability, we believe that the excessively large value we find for R is a result of a tunneling probability which is actually larger than the expression in Eq. (5) by some constant factor. This situation is often encountered in tunneling phenomena: it is difficult to predict the absolute value of tunneling currents, whereas its variation with parameters such as barrier height and barrier width can be calculated accurately. Though our model gives a tunneling current which is too low, the electric field and temperature dependence is in excellent agreement with the data. Assuming that a constant factor is missing in Eq. (5), we can compare the experimental values for the radii in He^4 and He^3:

$$\frac{R_3}{R_4} = \frac{30.1}{24.8} = 1.21 .$$

In the simple bubble model one has $R \propto \sigma^{-1/4}$; hence[29]

$$\frac{R_3}{R_4} = \left(\frac{\sigma_4}{\sigma_3}\right)^{1/4} = 1.21 .$$

The bubble radii scale exactly as predicted by the bubble model. So far we have discussed the pure liquids only. Our results for the mixtures (see Table I and Fig. 8) are peculiar. At lower temperatures (< 1 °K) the data deviate from the straight lines in Fig. 8. Obviously, an additional temperature dependence shows up. It seems plausible that this behavior is caused by the condensation of He^3 atoms at the free liquid surface and at the walls of the bubble. From the experiments by Guo *et al.*,[30] one can conclude that the first layer of He^3 atoms at the free liquid surface is completed at ~0.9 °K for a concentration of ~10%. This will decrease α, because most of the electrons tunnel through only 2–3 atomic layers as can be inferred from an analysis of the divergence of the tunneling current in Eq. (3) (see Fig. 10). Simultaneously, R will become temperature dependent, since a similar condensation of He^3 atoms is supposed to occur at the walls of the bubble[31] (R will increase). These processes will increase the escape rate P, in qualitative agreement with our results (see Fig. 8). The observation, however, that the data for the 19.5% mixture finally lie above the pure He^3 data (see Fig. 8) might indicate that the entire escape mechanism changes (the temperatures are close to the phase-separation temperature of 0.47 °K).

The most peculiar feature of the data for the mixtures is their straight-line behavior at higher temperatures (> 1 °K), yielding a binding energy $E_1 - E_0$ which lies below that in He^3 and a radius R below that in He^4. For example, the 12% mixture should have a negligible He^3 surface condensation at these temperatures. A straight-line behavior is shown in Fig. 8 over eight orders of magnitude.

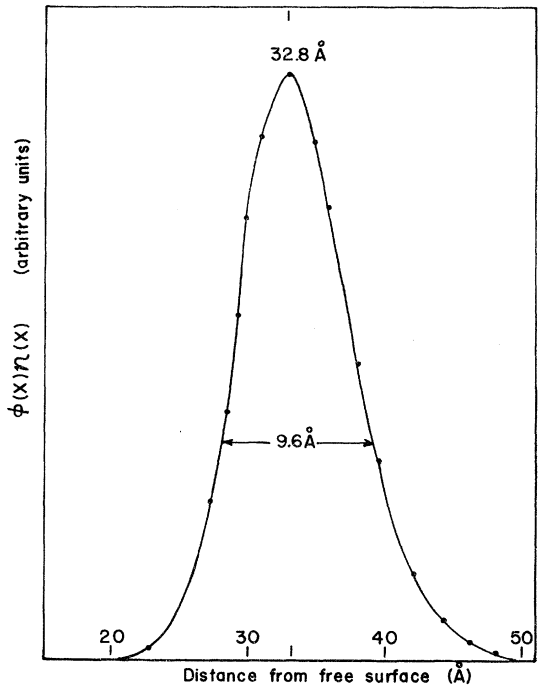

FIG. 10. Divergence of the tunneling current $\phi(x)n(x)$ as a function of distance from the free surface for pure He^4 with $\mathcal{E} = 150$ V/cm and $T = 1.0$ °K. The position of the maximum depends on $\mathcal{E}$ and T.

Presently, no reason is available to suggest that the binding energy of a bubble state in a He^3-He^4 mixture might actually be lower than that in pure He^3. Instead, we can only speculate that an additional temperature dependence [e.g., $R(T) = R_0 + R_1/\sqrt{T}$] might exist, which in our plot would still give a straight-line behavior, with a different slope. The intercept of the straight lines would then be determined by the temperature-independent part of R.

We conclude this section with a discussion of the assumptions we have made in our tunneling model. We assumed that the bubble remains spherical even in the strong and inhomogeneous electric field of the image charge. This can be justified by comparing the force $\vec{f}$ exerted by the electron on the walls of the bubble with the image force acting on the electron. The equilibrium radius of the bubble is determined by a cancellation of the pressure of the electron and the pressure due to the curvature of the bubble surface:

$$f/4\pi R^2 = 2\sigma/R \ .$$

Hence

$$f = 8\pi R\sigma = 87.4\ ^\circ\mathrm{K\ \AA^{-1}} \quad \text{for } R = 16\ \text{Å} \ .$$

On the other hand, the total image force on the electron located at $x = 25$ Å below the surface is only

$$\frac{A}{x^2} = \frac{1099}{(25)^2}\ ^\circ\mathrm{K\ \AA^{-1}} = 1.8\ ^\circ\mathrm{K\ \AA^{-1}} \ .$$

The bubble therefore will remain spherical. We also assumed that the image force acting on the liquid-vapor interface would not disturb the planar surface appreciably. This effect can be estimated by comparing the pressure produced by the induced surface charge density ω_p in the presence of the Coulomb field $\mathcal{E}_0$ of the electron with the pressure of a curved surface $2\sigma/r$, where r is the radius of curvature:

$$\frac{2\sigma}{r} \sim \mathcal{E}_0\omega_p = \frac{e}{\epsilon x^2}\ \frac{e(\epsilon-1)}{2\pi(\epsilon+1)x^2} = \frac{4A}{2\pi x^4} \ .$$

We have used the maximum value of ω_p, which exists right above the electron. Hence the maximum curvature is

$$r \approx \pi\sigma x^4/A \ .$$

Since most of the tunneling takes place at distances x larger than 25 Å, r will always be greater than 100 Å. The curvature of the surface therefore can be neglected. This can be concluded also from the good agreement between the calculated and the experimental values for A. The assumption of a rectangular square-well potential for the bubble and a discontinuous density change at the liquid surface as shown in Fig. 2 is clearly an oversimplification of the actual situation of a continuous density profile. Unfortunately, this density variation is not yet known accurately enough to incorporate it in our model. It is, however, obvious that a finite density profile would enhance the tunneling probability. One might try varying the density profile to fit our measured escape rates. But in agreement with what we have said earlier, the result will remain uncertain because of the general difficulty in predicting the absolute values of tunneling currents correctly. Finally, it should be mentioned that our model is a semiclassical treatment of the tunnel effect. A more rigorous theoretical calculation which includes a more detailed picture of the barrier[32] would be desirable.

VI. CONCLUSIONS

We have demonstrated that the transport of electrons through the free surface of liquid helium can be described as a tunnel effect from the electronic bubble state into the vapor phase. From the measured escape rates, the binding energy and (to a lesser extent) the radius of the bubble state can be determined. Our results for the binding energies in He^4 and He^3 are in good agreement with a recent calculation by Fetter based on an optical model. The radii in both liquids scale according to the prediction of a simple bubble model; however, their absolute values are too large. We obtained peculiar results in two He^3-He^4 mixtures which we cannot explain presently.[33] Our method is applicable to all dielectric liquids in which electronic bubble states exist with a positive ground-state energy; neon and hydrogen appear to be promising candidates for future study.

ACKNOWLEDGMENTS

It is a pleasure to thankfully acknowledge valuable discussions with A. L. Fetter, J. Lekner, G. Mahan, and R. M. Mazo. We are grateful to R. P. Mitchell for his stimulating interest and to H. Birdseye and V. Srinivasan for experimental help. One of us (W.S.) is thankful to the Deutscher Akademischer Austauschdienst for granting him a NATO postdoctoral fellowship and to the members of the Department of Physics of the University of Oregon for the hospitality extended to him.

APPENDIX

A brief discussion of the particle distribution inside the image-induced potential well $V(x) = A/x + e\mathcal{E}x$ is now presented. Assuming conditions inside the well are such that the distribution of ions $n(x, t)$ can be discussed in terms of the diffusion equation, we have

$$\frac{\partial n(x,t)}{\partial t} = \frac{\partial}{\partial x}\left(D\frac{\partial n}{\partial x} + \frac{D}{T}V'(x)n(x,t)\right) - \phi(x)n(x,t) \ , \tag{8}$$

with

$$V'(x)=\frac{dV}{dx}=-\frac{A}{x^2}+e\mathcal{E}\ ,\quad \phi(x)=\tfrac{1}{2}\nu e^{2\alpha R}\,W(x)$$

[see Eq. (2)], and D being the diffusion coefficient of the particles.

This equation is sometimes called the Smoluchowsi equation[13] and in our case includes a loss term $[\phi(x)n(x,t)]$ due to tunneling.

We have attempted to find an analytical solution to this equation and have been unsuccessful. Great difficulty is encountered, owing to the second-order pole at $x=0$.

The general form of the equation allows separation of variables. Using $n(x,t)=X(x)T(t)$ and substituting into Eq. (8) yields

$$-PX_p=\frac{d}{dx}\left(D\frac{dX_p}{dx}+\frac{D}{T}V'(x)X_p(x)\right)-\phi(x)X_p(x)\ ,$$
$$-PT_p(t)=\frac{d}{dt}T_p(t)\quad\text{or}\quad T_p(t)=e^{-Pt}\ , \tag{9}$$

with $-P$ being the separation constant.

Equation (9) may be recognized as a special form of the general Sturm–Liouville equation:

$$\frac{d}{dx}\left(r(x)\frac{dX_p}{dx}\right)+[q(x)+Pf(x)]X_p=0\ , \tag{10}$$

where

$$r(x)=e^{V(x)/T}\ ,$$
$$q(x)=\left(\frac{V''_{(x)}}{T}-\frac{\phi(x)}{D}\right)r(x)\ ,$$
$$f(x)=(1/D)\,r(x)\ ,$$

and P is the eigenvalue corresponding to the eigenfunction X_p. If $\phi(x)=0$, then the eigenfunction $X_p(x)=e^{-V(x)/T}$ (Maxwell–Boltzmann distribution) has as its eigenvalue $P=0$ (no particles escape from the well); if $\phi(x)$ is "small," then a first-order approximation to the eigenvalue P may be found using the unperturbed eigenfunction $X_0(x)=e^{-V(x)/T}$. We have by substituting into (9) and integrating

$$\int_0^\infty \phi(x)X_0(x)\,dx=P\int_0^\infty X_0(x)\,dx\ ;$$

then

$$P=\frac{\int_0^\infty \phi(x)e^{-V(x)/T}\,dx}{\int_0^\infty e^{-V(x)/T}\,dx}\ ,$$

which is essentially Eq. (3) in the text.

A direct solution of Eq. (9) for the eigenfunction is again hindered by the pole in $V(x)$. A variational technique may give a better approximation to the eigenvalue P than the one we have used in the text. Deep inside the liquid, $\phi(x)$ vanishes and the Maxwell–Boltzmann distribution should be quite good. The electric field and temperature dependence of the measured escape rate P from the surface is in very good agreement with our approximate solution and the observation that the current from the surface decays exponentially once the source of ions is turned off.

A numerical solution of Eq. (8) on a computer should be possible and we are investigating this approach.

---

*New address: Fachbereich Physik, Universität Regensburg, D-84 Regensburg, Germany.

†Alfred P. Sloan Fellow, supported by the National Science Foundation under Grant No. GP-29659.

[1]A. L. Fetter, in *The Physics of Liquid and Solid Helium*, edited by K. H. Batemann and J. B. Ketterson (Wiley, New York, to be published).

[2]F. Reif and L. Meyer, Phys. Rev. 119, 1165 (1960); see also Ref. 1.

[3]W. P. Pratt, Jr. and W. Zimmerman, Jr., Phys. Rev. 117, 412 (1969); see also Ref. 1 (Sec. IV).

[4]J. A. Northby and T. M. Sanders, Jr., Phys. Rev. Lett. 18, 1184 (1967); C. Zipfel, Ph.D. thesis (University of Michigan, 1969) (unpublished).

[5]G. Careri, U. Fasoli, and F. S. Gaeta, Nuovo Cimento 15, 774 (1960).

[6]L. Bruschi, B. Maraviglia, and F. Moss, Phys. Rev. Lett. 17, 682 (1966).

[7]W. Schoepe, and C. Probst, Phys. Lett. A 31, 490 (1970); and *Proceedings of the Twelfth International Conference on Low Temperature Physics*, edited by E. Kanda (Keigaku Publishing Co., Tokyo, 1971).

[8]G. W. Rayfield and W. Schoepe, Phys. Lett. A 31, 133 (1971); and Z. Naturforschung A 26, 1392 (1971).

[9]G. W. Rayfield and W. Schoepe, Phys. Lett. A 37, 417 (1971).

[10]G. W. Rayfield and W. Schoepe, Proceedings of the Thirteenth International Conference on Low Temperature Physics (Boulder, 1972) (unpublished).

[11]We use the WKB approximation and do not attempt to match boundary conditions for the electronic wave function.

[12]Jahnke-Emde-Lösch, *Tables of Higher Functions* (Teubner Velagsgesellschaft, Stuttgart, 1960), p. 18.

[13]The same argument is generally used in the calculation of the escape of Brownian particles over a high potential barrier; see e.g., H. A. Kramers, Physica 7, 184 (1940); see also S. Chandrasekhar, in *Selected Papers on Noise and Stochastic Processes*, edited by N. Wax (Dover, New York, 1954).

[14]I. S. Gradshteyn and I. M. Ryzhik, *Tables of Integrals Series and Products* (Academic, New York, 1965).

[15]*Handbook of Mathematical Functions*, Natl. Bur. Stds. Applied Mathematics Series, No. 55 (U. S. GPO, Washington, D. C., 1966).

[16]The dielectric constant of He^4 $\epsilon=1.057$ was taken from *Properties of Materials at Low Temperatures*, edited by V. J. Johnson (Pergamon, Oxford, 1961).

[17]A numerical error in Ref. 9 led to an incorrect value for R.

[18]The dielectric constant of He^3 was calculated to be $\epsilon=1.042$; see E. C. Kerr and R. H. Sherman, in *Pro-*

ceedings of the Eleventh International Conference on Low Temperature Physics, edited by J. F. Allen, D. M. Finlayson, and D. M. McCall (St. Andrews, 1968), p. 236.

[19]In Ref. 10 an attempt was made to derive A from a plot of lnP vs $\sqrt{\delta}$ at fixed T. Because of the few data points involved, that fit is much less accurate than the present one and may result in apparent discrepancies.

[20]B. Burdick, Phys. Rev. Lett. 14, 11 (1965).

[21]J. Jortner, N. R. Kestner, S. A. Rice, and M. H. Cohen, J. Chem. Phys. 43, 2614 (1965).

[22]J. L. Levine and T. M. Sanders, Jr., Phys. Rev. 154, 138 (1967).

[23]T. P. Eggarter, Phys. Rev. A 5, 2496 (1972).

[24]A. L. Fetter, private communication; see also Ref. 1 (Sec. III).

[25]W. T. Sommer, Phys. Rev. Lett. 12, 271 (1964).

[26]M. A. Woolf and G. W. Rayfield, Phys. Rev. Lett. 15, 235 (1965).

[27]T. Miyakawa and D. L. Dexter, Phys. Rev. A 1, 513 (1970).

[28]R. P. Mitchell and G. W. Rayfield, Phys. Rev. Lett. 42A, 267 (1972).

[29]The surface tensions of He^4 and He^3 were taken from J. Wilks, *The Properties of Liquid and Solid Helium* (Clarendon, Oxford, 1967), p. 422.

[30]H. M. Guo, D. O. Edwards, R. E. Sarwinski, and J. T. Tough, Phys. Rev. Lett. 27, 1259 (1971).

[31]G. W. Rayfield, Phys. Rev. Lett. 20, 1467 (1968); A. J. Dahm, Phys. Rev. 180, 259 (1969).

[32]The barrier through which the electron tunnels is only two to three layers thick. Since the electron "moves" much faster than the He atoms, fluctuations in the barrier are "visible" to it. In addition, it remains unclear to what extent the stored surface energy of the bubble $4\pi R^2$ contributes to the tunneling probability, as kindly pointed out to us by H. W. Lefevre.

[33]Some rather interesting results were also obtained for low liquid levels (2 mm) in pure He^4. For $T<0.9$ K *both* positive and negative charges were observed to emerge from the surface. The current was *not* related to photoemission from metal surfaces in the vapor phase observed earlier (see Ref. 8) but might be related to the neutral excitation discovered by C. M. Surko and R. Reif [Phys. Rev. 175, 229 (1968)] at lower temperatures and higher liquid levels. This phenomenon is presently under further investigation.

PHYSICAL REVIEW A VOLUME 7, NUMBER 6 JUNE 1973

Distribution of the Time-Dependent Microfield in a Plasma*

Larry J. Roszman
Institute for Basic Standards, National Bureau of Standards, Washington, D. C. 20234

C. F. Hooper, Jr.
Physics Department, University of Florida, Gainesville, Florida 32601

(Received 19 January 1973)

The theory of the distribution of the time average of the time-dependent microfield in a quantum plasma taken over a finite time interval is introduced and developed. The short- and long-time limits are derived. The Wigner phase-space representation is employed to derive the correct distribution for a classical plasma and to establish a formalism which can be used for low-order quantum corrections. Numerical results are presented for a classical gas of charged noninteracting particles. It is found that for time-averaging intervals, which are larger than the time it takes a particle traveling with the average thermal velocity to cross the ion-sphere radius, the distribution deviates from the corresponding Holtsmark distribution for the quasistatic model.

I. INTRODUCTION

The work reported here is an investigation of the distribution of the time average of the low-frequency component (ion produced) of the time-dependent microfield in a plasma taken over a finite time interval. While the distribution of the static (time-independent) microfield has a rich history of development[1-3] and application,[4-8] the distribution of the time-dependent microfield has received significant attention only recently. Most investigations of the time-dependent microfield have dealt with the distribution of the instantaneous value of the microfield when it is relaxing from some initial value rather than with the distribution of the finite time integral of the field.[9-11] Though the particular distribution introduced here developed originally from a scalar-additivity theory of the effects of ion motion on spectral line broadening in plasmas,[12] it should have broader application, possibly in those experimental situations such as probe measurements, where fields at a point are determined over finite rather than infinitesimal time intervals.[13]

In Sec. II the quantum-mechanical version of this distribution is defined and its extreme time limits ($t\to 0, \infty$) are determined. The Wigner phase-space representation of the distribution is developed in Sec. III, and the classical limit is obtained in Sec. IV. The simple model of a charged ideal gas is